corrosion and materials degradation

MDPI

Article

Coffee Bioactives as an Efficient Mixed-Type Green Corrosion Inhibitor for Carbon Steel: Mechanism, Adsorption, and Surface Analysis

Mohamed A. Deyab [1,*] and Q. Mohsen [2]

[1] Egyptian Petroleum Research Institute (EPRI), Nasr City, Cairo 11727, Egypt
[2] Department of Chemistry, College of Science, Taif University, Taif 21944, Saudi Arabia
* Correspondence: hamadadeiab@yahoo.com; Tel.: +20-1006137150

Abstract

This study investigates the corrosion inhibition performance of a sustainable green extract derived from Spent Coffee Silverskin (SCS) using ultrasound-assisted extraction (UAE). High-performance liquid chromatography (HPLC) quantified Caffeine (43.9 mg/g), α-Tocopherol (36.69 mg/g), Chlorogenic acid (6.9 mg/g), and Hyperoside (4.98 mg/g) as the primary bioactive ingredients. Weight loss metrics showed a dramatic drop in corrosion rate from 4.35 mg cm^{-2} h^{-1} (blank) to 0.28 mg cm^{-2} h^{-1} at the optimum concentration of 300 mg L^{-1} in a highly aggressive 1.0 M HCl environment, delivering a maximum efficiency of 93.5% at 298 K. Extended immersion tests proved remarkable short-term stability of the protective phytochemical film, maintaining an inhibition efficiency of 92.1% after 48 h of continuous exposure in the aggressive acidic medium. For comparison across techniques, maximum inhibition efficiencies of 95.4% and 96.8% were obtained from potentiodynamic polarization and electrochemical impedance spectroscopy (EIS), respectively. Importantly, these values are strictly method-dependent, reflecting the distinct physical parameters measured by each technique, and do not imply direct equivalence. Potentiodynamic polarization curves revealed mixed-type inhibitor characteristics, suppressing both anodic iron dissolution and cathodic hydrogen evolution. Notably, the corrosion current density (j_{corr}) dropped from 521.00 to 23.97 uA cm^{-2}, while the shift in the corrosion potential (E_{corr}) remained within 50 mV. EIS studies confirmed charge-transfer control, showing a rise in charge transfer resistance (R_{ct}) from 23.3 to 728.0 ohm.cm^2 paired with a drop in constant phase element (CPE) values from 642 to 218 uF cm^{-2}, demonstrating the displacement of surface water molecules by a dense, protective organic film. Thermodynamic evaluation indicated a drop in efficiency at elevated temperatures (90.7% at 328 K) alongside an increase in activation energy (E_a) from 9.99 to 20.16 kJ mol^{-1}. Adsorption behaviour strictly obeyed the Freundlich isotherm with the standard Gibbs free energy of adsorption (ΔG^o_{ads}) −17.35 kJ mol^{-1}. Scanning electron microscopy (SEM) visually confirmed a remarkably smooth and uniform protected metal surface, free from the severe pitting and deep cracks seen in the blank. Energy-dispersive X-ray (EDX) spectroscopy mathematically backed this visual barrier, showing a drop in oxygen content from 28.55% to 3.35%, alongside a sharp rise in surface carbon (10.55%) and nitrogen (1.69%) originating from the adsorbed phytochemical network. Density Functional Theory (DFT) modeling supported the inhibition mechanism at the molecular level, confirming Hyperoside and Chlorogenic acid as the driving reactive variants for electron transfer and iron d-orbital coordinate bonding.

Check for updates

Academic Editor: Ime Bassey Obot

Received: 7 September 2026
Revised: 2 October 2026
Accepted: 5 October 2026
Published: 15 October 2026

Copyright: © 2026 by the authors. Licensee MDPI, Basel, Switzerland. This article is an open access article distributed under the terms and conditions of the Creative Commons Attribution (CC BY) license.

Keywords: coffee extract; green corrosion inhibitor; adsorption; density functional theory (DFT); carbon steel degradation

1. Introduction

Corrosion of metallic structures is a significant industrial challenge [1], leading to massive economic losses and safety hazards, particularly in industries involving acid cleaning [2], industrial descaling, and oil well acidification [3]. Carbon steel is widely utilized in these sectors due to its excellent mechanical properties and cost-effectiveness [4]. However, it is highly susceptible to aggressive attack in acidic media, such as1.0 M HCl [5], which promotes rapid metal dissolution and hydrogen evolution [6]. To mitigate this, corrosion inhibitors are commonly employed [7]. While synthetic chemical inhibitors (often containing sulfur, nitrogen, and oxygen) are effective [8], many are toxic, expensive, and non-biodegradable, posing severe risks to the environment and human health [9,10]. Consequently, there is a global shift toward the development of "Green Corrosion Inhibitors" [11,12]. Plant extracts have emerged as a promising alternative because they are renewable, eco-friendly, and contain a rich variety of phytochemicals—such as polyphenols, flavonoids, and alkaloids—that possess lone pairs of electrons and aromatic rings ideal for adsorption onto metal surfaces [13,14].

While the utilization of crude plant extracts as green corrosion inhibitors for steel in 1.0 M HCl is widely documented, the vast majority of existing literature relies on empirical, phenomenological screening of unrefined mixtures. This creates a critical knowledge gap regarding the specific molecular drivers and the long-term structural durability of such films. To address these limitations, this study provides a highly targeted, mechanistically driven evaluation of a sustainable coffee extract (SCS) isolated via ultrasound-assisted extraction (UAE). Moving beyond conventional screening, this work uniquely integrates high-performance liquid chromatography (HPLC) to quantify the primary bioactive constituents. The core novelty o this study lies in the investigation of SCS extract as a high-performance bio-inhibitor. While many natural extracts lose their effectiveness at elevated temperatures, this work demonstrates that the protective film formed by SCS extract remains stable and highly efficient even at 328 K. Utilizing Spent Coffee Silverskin (SCS) as a corrosion inhibitor represents a dual-purpose strategy: it addresses the environmental burden of coffee industry waste while providing a low-cost, high-performance green inhibitor. While coffee grounds have been studied previously, the silverskin is a more concentrated source of thermally stable antioxidants. This study is among the first to demonstrate that SCS constituents can achieve a chemisorption-dominant bond on carbon steel, providing superior protection in aggressive acidic environments.

While previous literature has successfully evaluated coffee as waste-derived inhibitors [15], those systems typically report a multi-component matrix effect dominated by complex melanoidins, frequently limited to simple physical adsorption mechanisms. This study explicitly differentiates itself by targeting Spent Coffee Silverskin (SCS)—a dry roasting by-product rather than a wet brewing residue. By pairing precise HPLC profiling with Density Functional Theory (DFT) modeling, this work provides a definitive molecular-level look at the mechanism.

In this research, the inhibitory effect of SCS extract on carbon steel in 1.0 M HCl is comprehensively evaluated using weight loss analysis, potentiodynamic polarization (Tafel), EIS, and thermodynamic modeling. Additionally, the surface integrity and elemental composition of the protected steel are verified through scanning electron microscopy (SEM)

and energy-dispersive X-ray spectroscopy (EDX) to elucidate the relationship between the extract's chemical structure and its anti-corrosive performance.

2. Materials and Methods

2.1. Materials and Medium

The corrosion tests were performed on carbon steel specimens with the following chemical composition (wt.%): 0.18% C, 0.36% Mn, 0.03% P, 0.02% S, and Fe balance. For weight loss measurements, the specimens were cut into dimensions of 3.0 × 3.0 × 0.2 cm. Before each experiment, the metal surfaces were mechanically polished with various grades of emery paper (up to 1200 grade), rinsed with distilled water, degreased with acetone, and dried in air. The corrosive medium,1.0 M HCl, was prepared by diluting analytical-grade 37% HCl with double-distilled water.

2.2. Preparation of SCS Extract

The SCS was dried in a ventilated oven (50 °C for 6 h) until a moisture content of approximately 5% was reached. The dried skin was ground into a fine powder using a laboratory mill and sieved to ensure particle uniformity. Briefly, 1 g of SCS powder was extracted with 50 mL of an ethanol/water mixture (80:20, v/v). Ultrasound-assisted extraction (UAE) was performed in an ultrasonic bath at 60 °C for 30 min at a frequency of 59 kHz. Following extraction, the mixture was centrifuged at 6000 rpm for 10 min (20 °C) to separate the solid residue. The supernatant was filtered through a 0.45 µm PTFE membrane filter and stored at −20 °C in the dark until further analysis.

All subsequent inhibitor working concentrations (e.g., 300 mg L^{-1}) refer strictly to the mass of this dry solid extract dissolved directly into the 1.0 M HCl testing medium.

The primary bioactive compounds in SCS were determined by Shimadzu HPLC model (Kyoto, Japan) (see Table 1). The HPLC system was equipped with a C18 reversed-phase column (250 mm × 4.6 mm, 5 µm) and a UV-Vis detector. The mobile phase consisted of a gradient mixture of 0.1% formic acid in water and acetonitrile at a constant flow rate of 1.0 mL min^{-1} at a column temperature of 298 K. Quantitation of the primary phytochemical constituents was performed using external calibration standards of caffeine and chlorogenic acid prepared across a concentration range of 5–100 mg L^{-1}, yielding linear calibration curves with correlation coefficients greater than 0.999. The measurement uncertainties for peak area, retention times and quantified compounds were strictly maintained below ±2.5%.

Table 1. The primary bioactive compounds in SCS extracts.

Compound Class	Key Active Ingredients	Concentration (mg/g)
Alkaloids	Caffeine	43.9
Phenolic Acids	Chlorogenic acid (5-CQA)	6.9
Flavonoids	Hyperoside	4.98
Vitamins	α-Tocopherol (Vitamin E)	36.69

2.3. Weight Loss Measurements

Weight loss experiments were conducted in a glass beaker containing 100 mL of the test solution. The specimens were weighed using an analytical balance (accuracy ±0.1 mg) and then immersed in 1.0 M HCl without and with different concentrations of SCS extract for a period of 6 h at temperatures ranging from 298 K to 328 K. After immersion, the samples were cleaned according to ASTM G1-03 standards, dried, and reweighed.

Equations (1) and (2) were employed to calculate the corrosion rate (C_R) and inhibition efficiency (η_W%) [16,17]:

$$C_R = \frac{W}{A \times t} \quad (1)$$

$$\eta_W\% = \frac{C_{R0} - C_R}{C_{R0}} \times 100 \quad (2)$$

where W, A, and t are the weight loss, specimen area, and immersion time. The terms C_{R0} and C_R correspond to the corrosion rates obtained for the blank and inhibited electrolytes.

All experimental measurements, including corrosion rate C_R and inhibition efficiency η_W%, were performed in triplicate to ensure reproducibility. The results are reported as the mean ± standard deviation (SD).

2.4. Electrochemical Measurements

Potentiodynamic polarization (Tafel) tests were carried out using a standard three-electrode cell configuration consisting of carbon steel as the working electrode (WE), a saturated calomel electrode (SCE) as the reference electrode, and platinum foil as the counter electrode (CE). Before recording the Tafel curves, the WE was immersed in the test solution for 30 min at open-circuit potential (OCP) to reach a steady state. Polarization curves were recorded at a scan rate of 0.167 mV/s the potential range of −250 to +250 Mv relative to OCP. A Potentiostat/3000-Gamry (Warminster, PA, USA) was used for electrochemical measurements.

Equation (3) was employed to derive the inhibition efficiency (η_j%) from the collected polarization parameters [18,19]. Here, the corrosion current density in the presence of the inhibitor is labeled j_{corr} while $j_{corr(0)}$ represents the corrosion current density of the blank solution

$$\eta_j\% = \frac{j_{corr(0)} - j_{corr}}{j_{corr(0)}} \times 100 \quad (3)$$

All polarization parameters were performed in triplicate to ensure reproducibility.

EIS measurements were conducted at the open-circuit potential over a frequency range from 100 kHz to 10 mHz with an AC amplitude of 10 mV.

2.5. Surface Characterization (SEM/EDX)

The surface morphology of the carbon steel specimens after 6 h of immersion in 1.0 M HCl (blank and 300 mg L^{-1} SCS extract) was analyzed using a scanning electron microscope (SEM, ZEISS EVO) (Oberkochen, Germany). The elemental composition of the protective film formed on the surface was further investigated using Energy-Dispersive X-ray Spectroscopy (EDX) (Carl Zeiss, Oberkochen, Germany).

2.6. Density Functional Theory (DFT) Calculations

Density Functional Theory (DFT) calculations performed on key active constituents (Caffeine, Chlorogenic acid, Hyperoside, and α-Tocopherol) were conducted using the DMol3 module within Materials Studio 6.0 (Accelrys). To replicate the aggressive 1.0 M HCl testing environment, the calculations were not performed in the gas phase; instead, an aqueous solvent model was incorporated using the Conductor-like Screening Model (COSMO).

3. Results and Discussion

3.1. Weight Loss Studies

Based on the data in Table 2, the significant decrease in the corrosion rate (C_R) from 4.35 mg cm^{-2} h^{-1} (blank) to 0.28 mg cm^{-2} h^{-1} at 300 mg L^{-1} indicates that the SCS extractacts as an effective "green" corrosion inhibitor. This behavior is typically attributed

to the adsorption of phytochemical constituents (like polyphenols, flavonoids, or alkaloids) onto the carbon steel surface [20–22]. These molecules form a protective film that masks the active sites, creating a physical barrier that prevents the aggressive1.0 M HCl ions from attacking the metal.

Table 2. Corrosion rates (C_R) and inhibition efficiency (η_W%) for carbon steel immersed in 1.0 M HCl at 298 K at different SCS extract concentrations.

SCS Extract	C_R	η_W%
(mg L^{-1})	(mg cm^{-2} h^{-1})	
Blank	4.35 ± 0.06	-
50	3.41 ± 0.13	21.6 ± 3.2
100	2.90 ± 0.09	33.3 ± 2.3
150	2.19 ± 0.14	49.7 ± 3.3
200	1.38 ± 0.05	68.3 ± 1.2
250	0.43 ± 0.03	90.1 ± 0.7
300	0.28 ± 0.02	93.6 ± 0.5

The relationship between concentration and efficiency isdirectly proportional. At the lowest concentration (50 mg L^{-1}), the inhibition efficiency (η_W%) is relatively low at 21.5%. However, as the concentration increases to 250 mg L^{-1}, there is a sharp jump in efficiency to 90.2%. This indicates that a critical concentration is reached where the metal surface becomes almost entirely covered by the inhibitor molecules. The leap in efficiency between 200 mg L^{-1} (68.2%) and 250 mg L^{-1} (90.2%) confirms a shift toward a more stable and compact protective layer at higher dosages. The maximum efficiency of 93.5% at 300 mg L^{-1} demonstrates that SCS extract is a highly potent inhibitor for acidic environments. Because high efficiency is achieved at relatively low concentrations (300 mg L^{-1}), the extract proves to be a cost-effective and eco-friendly alternative to synthetic chemical inhibitors.

To evaluate the short-term chemical stability and persistence of the protective film, weight loss measurements were performed at extended immersion periods of 12, 24, and 48 h using the optimum concentration of 300 mg L^{-1} SCS extract at 298 K. The resulting inhibition efficiencies are compiled in Table 3.

Table 3. The inhibition efficiency (η_W%) for carbon steel immersed in 1.0 M HCl containing 300 mg L^{-1} SCS extract at 298 K at different immersion times.

Immersion Time (Hours)	η_W%
6	93.6 ± 0.5
12	94.2 ± 0.4
24	94.4 ± 0.5
48	92.1 ± 0.6

As the immersion time increases from 6 to 24 h, the inhibition efficiency exhibits an exceptionally stable plateau, shifting marginally from 93.5% to a peak value of 94.4%. This performance profile indicates that the active phytochemical molecules (heteroatoms and π-electron systems) continue to safely migrate to the metal interface over time, filling any remaining active micro-voids. Instead of desorbing into the bulk solution, the adsorbed organic matrix undergoes surface consolidation, structural reorganization, and closer molecular packing. This yields a dense, hydrophobic barrier that strongly hinders

the diffusion of corrosive ions. Even after an extensive 48-h continuous exposure to the highly aggressive 1.0 M HCl environment, the protective matrix maintains an outstanding inhibition efficiency of 92.1%. While long-term structural applications require months of monitoring in milder environments, this 48-h stability highlights the exceptional performance of the SCS extract for short-term, high-intensity applications such as industrial acid pickling and chemical descaling.

3.2. Electrochemical Studies

The Tafel polarization curves in Figure 1 show the electrochemical behavior of carbon steel immersed in 1.0 M HCl at 298 K at different SCS extract concentrations. The extracted data are listed in Table 4. The polarization curves (Figure 1) show a clear shift in the Tafel plots toward lower current densities as the concentration of SCS extract increases. This indicates that the extract effectively hinders the movement of ions, thereby reducing the rate of the corrosion reaction. There is a dramatic reduction incorrosion current density (j_{corr}) from 521.00 μA cm^{-2} (blank) to 23.97 μA cm^{-2} at 300 mg L^{-1}. This confirms the high inhibition efficiency (η_j% =95.4), which aligns closely with your weight loss study results. The values of corrosion potential (E_{corr}) shift slightly toward the noble (more positive/anodic) direction, moving from −496 mV to −454 mV. Since the maximum displacement is approximately 42 mV (which is less than the standard 85 mV threshold), the SCS extract is classified as a mixed-type inhibitor [23]. This means it suppresses both the anodic metal dissolution and the cathodic hydrogen evolution reactions.

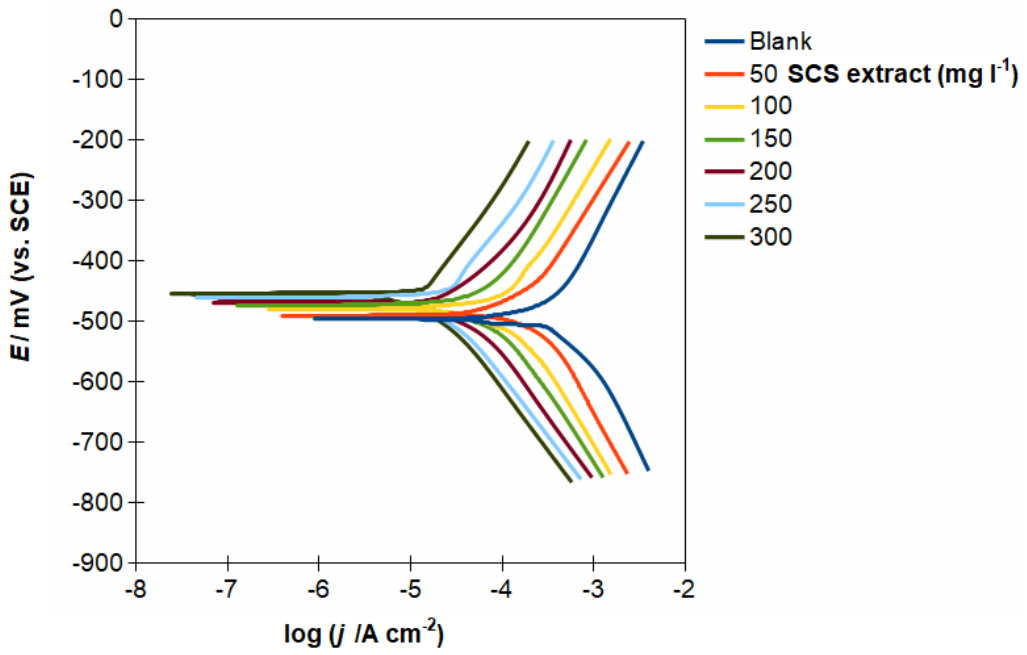


Figure 1. Polarization curves (Tafel type) for carbon steel immersed in 1.0 M HCl at 298 K at different SCS extract concentrations.

As presented in Table 4, the anodic Tafel slope (β_a) exhibits a noticeable decrease from 91 mV/dec in the blank solution to 73 mV/dec at the optimum inhibitor concentration—signifying a change of approximately 20%. Rather than reflecting simple geometric site blocking, this significant variation indicates that the adsorbed SCS constituents actively alter the anodic iron dissolution mechanism [24,25].

It is important to emphasize that while the calculated inhibition efficiencies from polarization and gravimetric methods are complementary; their absolute corrosion rates exhibit a clear numerical gap. This variance is fundamentally driven by exposure-time dy-

namics. Polarization captures an instantaneous, short-term charge-transfer current density before extensive surface microstructural degradation occurs. In contrast, the weight-loss methodology integrates cumulative mass destruction over a prolonged immersion window. In the aggressive 1.0 M HCl medium, localized chloride attack triggers autocatalytic pitting and grain boundary degradation over time. This long-term degradation accelerates the macroscopic mass loss, yielding higher absolute corrosion rates than those calculated theoretically via short-term electrochemical tracking.

Table 4. Polarization parameters for carbon steel immersed in 1.0 M HCl at 298 K at different SCS extract concentrations.

SCS Extract	$E_{corr.}$	j_{corr}	β_a	$-\beta_c$	η_j%
(mg L^{-1})	mV (SCE)	μA cm^{-2}	(mV dec^{-1})	(mV dec^{-1})	
Blank	−496	521.00	91	133	-
50	−490	398.04	90	134	23.6
100	−480	337.61	87	123	35.2
150	−473	244.35	82	122	53.1
200	−468	150.05	79	120	71.2
250	−461	40.12	79	119	92.3
300	−454	23.97	73	120	95.4

As observed in Figure 2a, the Nyquist plots exhibit a single capacitive loop across the studied frequency range.

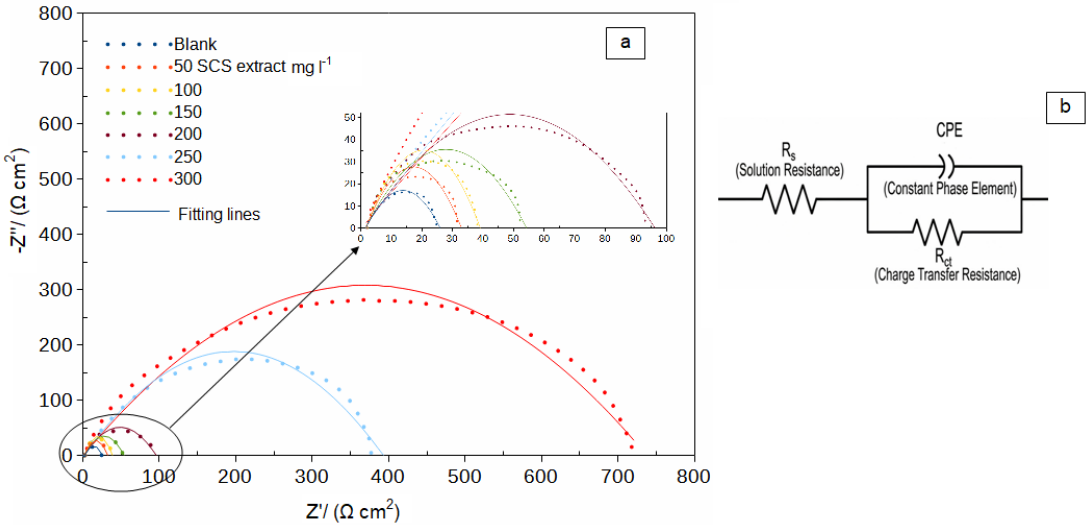


Figure 2. (**a**) Nyquist curves for carbon steel immersed in 1.0 M HCl at 298 K at different SCS extract concentrations; (**b**) the corresponding equivalent circuit model used for data fitting.

It is important to note that the presence of a single capacitive loop does not imply pure charge-transfer control alone. Because the sustainable SCS phytochemical network forms an ultra-thin molecular barrier, its corresponding film resistance (R_{film}) possesses a relaxation time constant that overlaps almost identically with that of the electrical double layer ($R_{ct,true}$). As a result, these individual sub-processes cannot be resolved into separate arcs and instead merge into a single, comprehensive loop. Therefore, the calculated resistance parameter (R_{ct}) values reported in Table 5 are interpreted as a total interfacial polarization resistance ($R_{ct} = R_{ct,rue} + R_{film}$). Upon increasing the concentration of SCS extract from 50 to 300 mg L^{-1}, the diameter of the capacitive loops expands significantly.

The electrochemical parameters extracted from the circuit fitting Figure 2b, along with the calculated inhibition efficiency (η_R%), have been shown in Table 5.

$$\eta_R\% = \frac{R_{ct} - R_{cto}}{R_{ct}} \times 100 \quad (4)$$

where R_{ct0} and R_{ct} are the charge transfer resistances in the absence and presence of the SCS extract, respectively.

Table 5. EIS data for carbon steel immersed in 1.0 M HCl at 298 K at different SCS extract concentrations.

SCS Extract (mg L^{-1})	R_s (ohm.cm^2)	R_{ct} (ohm.cm^2)	C_{eff} (μF cm^{-2})	η_R%
Blank	1.7	23.3	642	-
50	1.6	31.2	602	25.3
100	1.2	36.8	511	36.6
150	1.3	49.4	489	52.8
200	1.0	92.0	462	74.6
250	1.1	375.8	322	93.8
300	1.1	728.0	218	96.8

Quantitatively (Table 5), the charge transfer resistance (R_{ct}) rises dramatically from 23.3 ohm.cm^2 (blank) to 728.0 ohm.cm^2 at 300 mg L^{-1}. This remarkable increase yields an inhibition efficiency (η_R%) of 96.8%. Concurrently, the converted effective double-layer capacitance (C_{eff}) values—derived from the constant phase element parameters (CPE) to accurately account for surface frequency dispersion—decrease significantly from 642 to 218 μF cm^{-2}. This dual effect, R_{ct} increase and C_{eff} decrease, provides clear evidence that the organic molecules within the SCS extract successfully adsorb onto the steel surface. This process displaces water molecules, reduces the local dielectric constant, and forms a dense, protective layer that isolates the metal surface from the aggressive (H^+) and (Cl^-) ions.

3.3. Effect of Temperature and Activation Parameters

Table 6 shows that as the temperature rises from 298 K to 328 K, the corrosion rate (C_R) increases for both the blank and inhibited solutions. However, the inhibition efficiency (η_W%) remains remarkably stable, only slightly decreasing from 93.5% to 90.7%. This minimal decline indicates that the SCS extract forms a robust protective film that is thermally stable even at higher temperatures, making it a reliable inhibitor for industrial processes involving heat.

To further understand the nature of the inhibition process, the temperature dependence of the corrosion rate was analyzed using the Arrhenius Equation (5) and the Transition State Equation (6) [26,27]:

$$C_R = Ae^{\frac{-E_a}{RT}} \quad (5)$$

$$C_R = \frac{RT}{Nh}\exp\left(\frac{\Delta S^*}{R}\right)\exp\left(\frac{-\Delta H^*}{RT}\right) \quad (6)$$

(h = Planck constant, N = 6.02214076 × 10^{23} mol^{-1}, and A = constant).

Figure 3a displays the Arrhenius plots for the carbon steel in 1.0 M HCl, both with and without 300 mg L^{-1} of SCS extract. The linear regression of these plots allowed for the calculation of the apparent activation energy (E_a), as presented in Table 7. The E_a value increased significantly from 9.99 kJ mol^{-1} for the blank solution to 20.16 kJ mol^{-1} in the

presence of SCS. This increase in activation energy indicates that the SCS extract molecules create a higher energy barrier for the corrosion reaction to occur [27,28]. Figure 3b shows the transition state plots. The values of the enthalpy of activation (ΔH^*) and the entropy of activation (ΔS^*) were derived from the slopes and intercepts of these lines, respectively. This significant increase in ΔH^* (7.39 kJ mol^{-1} for the blank and 17.57 kJ mol^{-1} for the inhibited solution) upon the addition of the sustainable inhibitor indicates that the formation of the protective organic film introduces a higher energetic barrier for the activated complex to stabilize at the surface [29]. Consequently, the charge-transfer and mass transport steps required to drive metal dissolution become more energetically demanding, confirming the strong kinetic retarding capability of the chemisorbed phytochemical network. The values for ΔS^* are negative in both systems (−187 J K^{-1} mol^{-1} and −196 J K^{-1} mol^{-1}). These negative values indicate that the activated complex in the rate-determining step represents anassociative processrather than a dissociative one. This indicates a decrease in disorder as the reactants transition to the activated state on the inhibited metal surface [30,31].

Table 6. The C_R and η_W% for carbon steel in 1.0 M HCl at various temperatures with and without 300 mg L^{-1} SCS extract.

Temperature (K)	Solution	C_R (mg cm^{-2} h^{-1})	η_W%
298	Blank 1.0 M HCl	4.35	-
	300 mg L^{-1} SCS extract	0.28	93.5
308	Blank 1.0 M HCl	4.88	-
	300 mg L^{-1} SCS extract	0.35	92.8
318	Blank 1.0 M HCl	5.27	-
	300 mg L^{-1} SCS extract	0.45	91.4
328	Blank 1.0 M HCl	6.37	-
	300 mg L^{-1} SCS extract	0.59	90.7

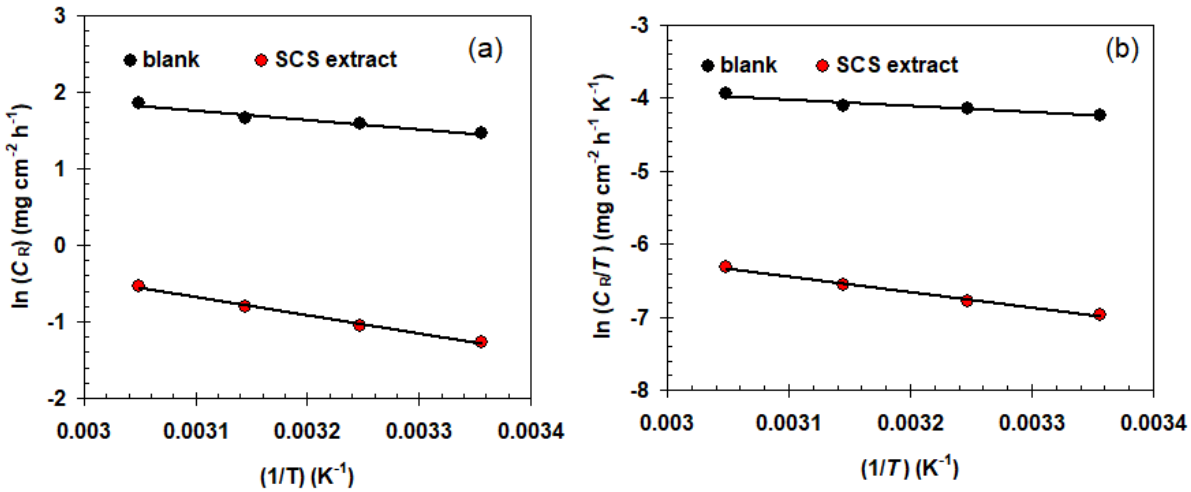


Figure 3. Arrhenius (**a**) and transition (**b**) plots for carbon steel in 1.0 M HCl with and without 300 mg L^{-1} SCS extract.

Table 7. Activation thermodynamic parameters for carbon steel in 1.0 M HCl with and without 300 mg L^{-1} SCS extract.

Solution	E_a (KJ mol^{-1})	ΔH^* (KJ mol^{-1})	ΔS^* (J K^{-1} mol^{-1})
1.0 M HCl	9.99	7.39	−187
1.0 M HCl + 300 mg L^{-1} SCS extract	20.16	17.57	−196

3.4. Adsorption Isotherm Studies

To understand the interaction between the SCS extract molecules and the carbon steel surface, the experimental data were fitted into several adsorption isotherms. The degree of surface coverage (θ) was calculated from the weight loss measurements using the relation:

$$\theta = \eta_W\%/100 \tag{7}$$

Figure 4 illustrates the fitting of the data to the Langmuir, Temkin, and Freundlich adsorption models at 298 K. The linear correlation coefficient (R^2) was used to determine the best-fit model [32]. The Langmuir model (as shown in Equation (8) and Figure 4a) yielded a low correlation coefficient (R^2 = 0.4149), suggesting that the adsorption of SCS extract does not follow the ideal Langmuir assumption of a monolayer on a fixed number of identical, independent sites. The Temkin model (as shown in Equation (9) and Figure 4b) showed a significantly better fit (R^2 = 0.9172), indicating the presence of lateral interactions between the adsorbed molecules or a non-uniform surface energy. The Freundlich isotherm (as shown in Equation (10) and Figure 4c) model provided the highest correlation coefficient (R^2 = 0.9841), indicating that the Freundlich isotherm is the best-fit modelfor describing the adsorption behavior of the SCS extract on the carbon steel surface.

$$\frac{C_{inh}}{\theta} = \frac{1}{K_{ads}} + C_{inh} \tag{8}$$

$$\exp(-2a\theta) = K_{ads}C_{inh} \tag{9}$$

$$\ln(\theta) = \ln K_{ads} + \frac{1}{n}\ln C_{inh} \tag{10}$$

where K_{ads} is the adsorption constant, "a" is the lateral interaction and "n" is a correction factor.

The superior fit of the Freundlich model indicates that the adsorption occurs on a heterogeneous surface with sites of varying adsorption energies. This is common for plant extracts, which are complex mixtures of various phytochemicals (such as polyphenols or alkaloids) that compete for different active sites on the steel surface.

The slope of the Freundlich plot ($1/n$) reflects both the adsorption intensity and the surface heterogeneity factor. In this study, the linear regression of the Freundlich isotherm yields a slope value of ($1/n$ = 0.87). Because this value falls strictly within the favorable adsorption range ($0 < 1/n < 1$), it mathematically establishes that the adsorption of the SCS extract onto the carbon steel surface is highly spontaneous and structurally favorable.

In this study, the high R^2 value confirms that the SCS extract molecules readily adsorb onto the metal surface, forming a stable protective film that effectively blocks the active sites from the corrosive 1.0 M HCl environment. From the intercept of Figure 4c, the K_{ads} value is about 0.006615 L/mg.

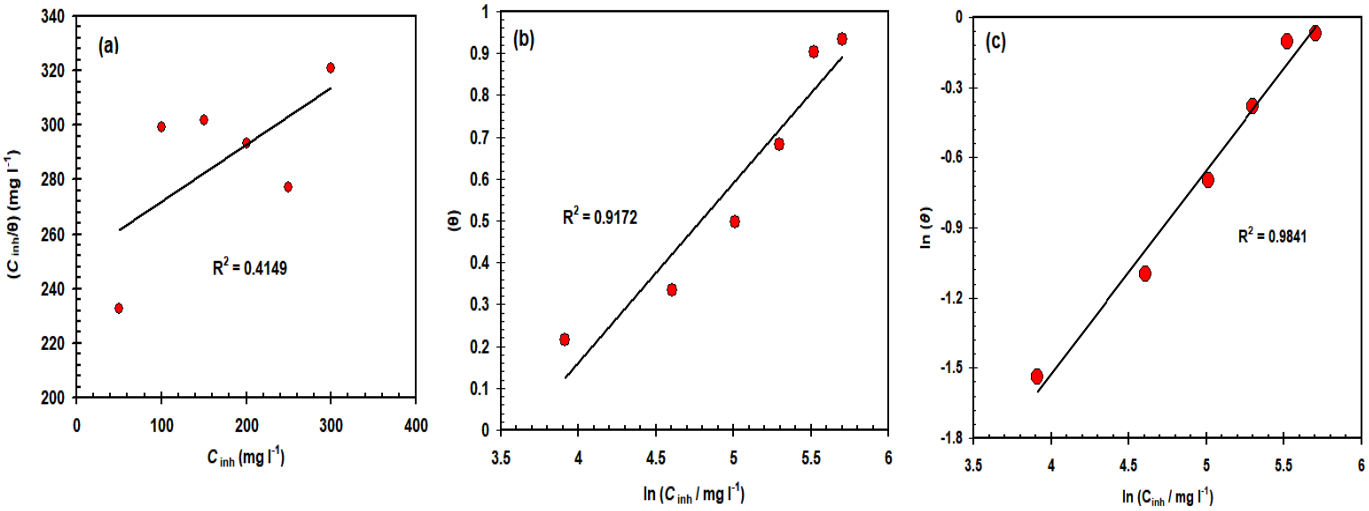


Figure 4. Adsorption isotherms for carbon steel in 1.0 M HCl solution containing SCS extract at 298 K: (**a**) Langmuir, (**b**) Temkin, and (**c**) Freundlich models.

The standard Gibbs free energy of adsorption (ΔG^{o}_{ads}) is calculated using the following thermodynamic relationship [33,34]:

$$\Delta G^{o}_{ads} = -RT \ln(10^6 \times K_{eq}) \quad (11)$$

where 10^6 is the concentration of water in mg/L, R = gas constant, and T = the absolute temperature.

To ensure absolute thermodynamic rigor and address the dimensional inconsistency of inserting an empirical parameter into a logarithmic identity, the empirical Freundlich constant (K_{ads} = 0.006615 L/mg) was converted into a standard dimensionless thermodynamic equilibrium constant (K_{eq}). The calculated value of ΔG^{o}_{ads} is −17.35 kJ mol^{-1}. The negative sign confirms that the adsorption of SCS extract onto the carbon steel surface is aspontaneous process [35].

3.5. Surface Morphology Analysis

To visually assess the protective effect of the SCS extract, the surface of the carbon steel was examined using SEM after immersion in 1.0 M HCl for 6 h. The micrographs are shown in Figure 5. In the case of the blank solution (1.0 M HCl only), the image (Figure 5a) reveals a highly damaged and degraded metal surface. The surface is characterized by severe pitting and cracks. The presence of deep pits and irregular cracks indicates a strong aggressive attack by the Cl^- and H^+ ions in the acid. Thick, uneven layers of corrosion products (likely iron oxides and chlorides) are visible, showing that the metal has undergone significant dissolution.

In the case of the inhibited solution (1.0 M HCl + 300 mg L^{-1} SCS extract), the image (Figure 5b) shows a remarkably smoother and more uniform surface. The severe pitting and deep cracks seen in the blank sample are almost entirely absent. Although minor surface features from the original metal polishing remain visible, the integrity of the surface is well-preserved. The smoother morphology is a direct suggestion of the formation of a stable, protective adsorption layer of SCS extract molecules. This structural trend correlates well with the high inhibition efficiencies and the significant reduction in corrosion current density determined in the electrochemical evaluations.

The elemental composition of the carbon steel surface was analyzed before and after the addition of the SCS extract to confirm the presence of the inhibitor film (in Table 8).

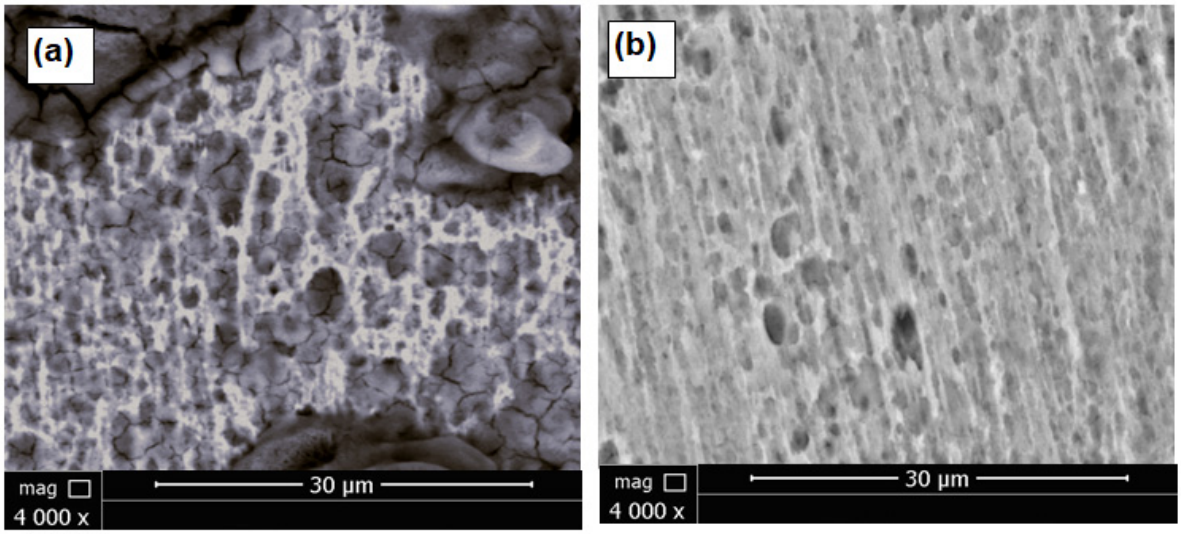


Figure 5. SEM image of carbon steel in 1.0 M HCl without (image (**a**)) and with 300 mg L^{-1} SCS extract (image (**b**)).

Table 8. Elemental composition (weight %) of carbon steel surface after 6 h immersion in 1.0 M HCl without (Blank) and with 300 mg L^{-1} SCS extract.

Sample	Fe	C	O	N	Cl
Carbon steel (Polished)	≈98.44	0.18	-	-	-
Blank (1.0 M HCl)	≈62.13	4.24	28.55	-	5.08
Inhibited (300 mg L^{-1} SCS)	≈84.38	10.55	3.35	1.69	0.03

It must be noted that EDX analysis operates as a semi-quantitative technique with inherent limitations when detecting light elements such as carbon (C) and nitrogen (N), primarily due to matrix absorption effects, low X-ray escape depths, and systematic hydrocarbon contamination common within electron microscope vacuum chambers. Therefore, the absolute weight percentages presented in Table 8 should be interpreted as relative surface trends rather than exact bulk values. In the absence of the inhibitor, the iron (Fe) percentage drops significantly, while a high percentage of oxygen (**O**) and chlorine (Cl) is detected. The high oxygen level (28.55%) indicates the extensive formation of iron oxides and hydroxides (rust), while the chlorine confirms the aggressive attack of the HCl medium. With the addition of 300 mg L^{-1} SCS extract, the iron signal remains high (84.38%) and the oxygen content is drastically reduced to 3.35%. This proves that the extract has successfully prevented the oxidation of the metal.

A key finding is the sharp increase in carbon (**C**) and the appearance of nitrogen (**N**) on the surface. Since these elements are not present in high amounts in the base metal, they originate from the phytochemical constituents of the SCS extract (such as alkaloids and polyphenols). The increased presence of organic elements (C, N) and the reduction in corrosion products (O, Cl) suggest that the SCS extract molecules have successfully adsorbed onto the steel surface, creating a robust organic barrier that shields the metal from the acidic environment.

3.6. Mechanism of Inhibition

The inhibition of carbon steel corrosion in 1.0 M HCl by CS extract is a complex process involving the displacement of water molecules (H_2O) by the organic constituents of the extract (SCS) [36–40]:

$$SCS_{(sol)} + nH_2O_{(ads)} \leftrightarrow SCS_{(ads)} + nH_2O_{(sol)} \quad (12)$$

The mechanism can be explained through three primary stages:

1. Adsorption of phytochemicals

The SCS extract contains various phytochemicals (such as Caffeine, and Vitamin E) characterized by the presence of heteroatoms (O, N) and π-electrons from aromatic rings. These act as active centers for adsorption. In the acidic 1.0 M HCl medium, heteroatoms can become protonated. These positively charged molecules attract the negatively charged chloride ions already adsorbed on the steel surface, forming an electrostatic bridge. This explains the increase inactivation energy (E_a). The lone pairs of electrons on Oxygen and Nitrogen atoms, along with the π-electrons of the aromatic rings, are transferred into the vacant d-orbitals of Fe atoms. The superior inhibition efficiency of SCS extract is the result of extract molecules' adsorption, creating a stable, multi-layered organic barrier that remains effective even as temperatures increase to 328 K.

2. Blocking of Active Sites

Once adsorbed, the extract molecules form a dense, hydrophobic protective film. This film performs two simultaneous roles:

- Anodic Suppression: It covers the active "nodes" where iron dissolution occurs ($Fe \rightarrow Fe^{2+} + 2e$), increasing the resistance to metal loss.
- Cathodic Suppression: It hinders the discharge of hydrogen ions ($2H^+ + 2e \rightarrow H_2$), thereby reducing the rate of hydrogen evolution.

This dual action confirms the mixed-type behavior observed in the Tafel polarization curves.

3. Steric Hindrance and Surface Protection

The large size of the organic molecules in the SCS extract provides a "steric hindrance" effect. A single molecule can cover a significant surface area, physically blocking the Cl^- and H^+ ions from reaching the metal. This is visually confirmed by the SEM images, which showed a smooth surface for the inhibited sample, and the EDX data, which showed a high carbon and nitrogen content on the protected steel.

3.7. Quantum Chemical Calculations (DFT)

To elucidate the inhibition mechanism at the molecular level, Density Functional Theory (DFT) calculations were utilized to analyze the electronic properties of the primary bioactive components of the SCS extract: Hyperoside, Chlorogenic acid (5-CQA), Caffeine, and α-Tocopherol.

All calculations were performed using the B3LYP hybrid functional combined with the split-valence 6-311++G(d,p) basis set. The Self-Consistent Field (SCF) energy convergence threshold was set to a tight tolerance of 1.0×10^{-8} a.u., with maximum force and displacement convergence criteria capped at 4.5×10^{-4} a.u. and 1.8×10^{-3} a.u., respectively. Furthermore, vibrational frequency calculations were systematically performed at the same level of theory to ensure the absence of imaginary frequencies. All calculated configurations yielded exclusively positive values well above the lower limit ($\nu > 0$ cm^{-1}), confirming that all molecules successfully attained their true ground-state structures.

The calculated Frontier Molecular Orbital (FMO) energies are summarized in Table 9 and Figure 6.

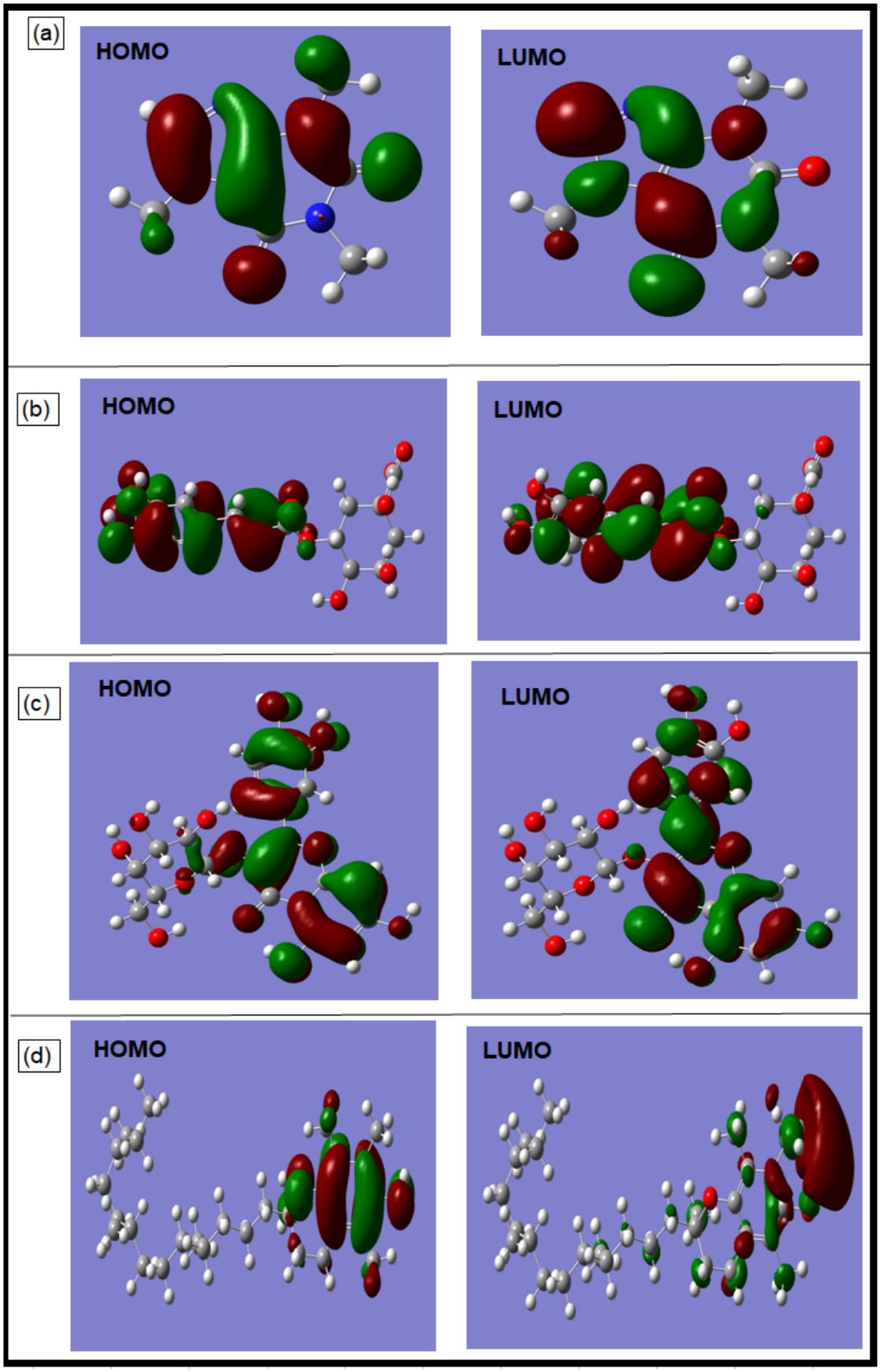


Figure 6. HOMO–LUMO for the key active constituents of SCS extract: (**a**) Caffeine, (**b**) Chlorogenic acid (5-CQA), (**c**) Hyperoside, and (**d**) α-Tocopherol (Vitamin E).

Table 9. Quantum chemical parameters for the key active ingredients of SCS extract.

Key Active Ingredients	E_{HOMO}/eV	E_{LUMO}/eV	ΔE/eV
Caffeine	−3.893	−0.872	3.021
Chlorogenic acid (5-CQA)	−3.205	−0.932	2.273
Hyperoside	−3.187	−1.243	1.944
α-Tocopherol (Vitamin E)	−4.021	−0.988	3.033

E_{HOMO} value is a measure of a molecule's tendency to donate electrons to an appropriate acceptor. In this study, the vacant d-orbitals of Fe atoms on the carbon steel surface act as the acceptors. Hyperoside (−3.187 eV) and Chlorogenic acid (−3.205 eV) exhibit the highest E_{HOMO} values; indicating they are the most potent electron donors in the extract. E_{LUMO} signifies the ability of the molecule to accept electrons from the metal surface (back-donation). Hyperoside (−1.243 eV) shows the lowest E_{LUMO}, suggesting it has the strongest capacity to accept electrons from the iron surface, thereby strengthening the adsorption bond.

The energy gap ($\Delta E = E_{LUMO} - E_{HOMO}$) is a vital parameter in predicting inhibition performance. A lower ΔE value implies that the molecule is more reactive and possesses a higher affinity for the metal surface. Hyperoside (1.944 eV) and Chlorogenic acid (2.273 eV) possess significantly lower energy gaps compared to the other constituents. This suggests that these polyphenols are the primary drivers of the high inhibition efficiency observed experimentally. The presence of Caffeine and α-Tocopherol, despite their higher gaps, supports the film's integrity through their heterocyclic nitrogen atoms and long-chain hydrophobic barriers, respectively. The high E_{HOMO} and low ΔE of the major SCS components facilitate the formation of coordinate-type bonds between the lone pairs of electrons (on O and N atoms) and the iron surface.

4. Conclusions

This study demonstrates that SCS extract is a highly efficient, green, and sustainable corrosion inhibitor for carbon steel in 1.0 M HCl. The following conclusions can be drawn:

1. The SCS extract shows outstanding mixed-mode inhibition properties, establishing a compact protective barrier on the carbon steel surface. The maximum protection efficiencies calculated from weight loss (93.5%), Tafel polarization (95.4%), and EIS measurements (96.8%) confirm excellent scientific agreement across all evaluation methods.
2. The adsorption of phytochemicals onto the steel surface obeys the Freundlich isotherm.
3. Tafel polarization and EIS data confirm that the SCS extract acts as a mixed-type inhibitor, effectively suppressing both the anodic dissolution of iron and the cathodic evolution of hydrogen.
4. The increase in activation energy (E_a) from 9.99 to 20.16 kJ mol^{-1} indicates the formation of a robust energy barrier. Despite a slight decrease in efficiency at higher temperatures, the extract maintains superior protection at 328 K.
5. Visual and elemental evidence from SEM and EDX confirm that the inhibitor creates a smooth, carbon-and-nitrogen-rich protective film that prevents pitting and surface degradation.
6. Overall, the SCS extract provides an effective and environmentally friendly alternative to synthetic inhibitors for industrial acid cleaning and pickling processes.

Author Contributions: Conceptualization, M.A.D. and Q.M.; methodology, M.A.D.; software, M.A.D. and Q.M.; validation, M.A.D.; formal analysis, M.A.D.; investigation, M.A.D.; resources, M.A.D.; data curation, M.A.D.; writing—original draft preparation, M.A.D.; writing—review and editing, M.A.D. and Q.M.; visualization, M.A.D.; supervision, M.A.D.; project administration, M.A.D.; funding acquisition, M.A.D. and Q.M. All authors have read and agreed to the published version of the manuscript.

Funding: This research was funded by the Deanship of Graduate Studies and Scientific Research at Taif University.

Data Availability Statement: The datasets used and/or analysed during the current study are available from the corresponding author on reasonable request.

Acknowledgments: The authors would like to acknowledge the Deanship of Graduate Studies and Scientific Research, Taif University for funding this work. During the preparation of this manuscript, the authors used a large language model (LLM), specifically the Google AI assistant, strictly for the purpose of language improving, proofreading, and refining English grammar and readability. After using this assistance, the authors thoroughly reviewed, edited, and revised the content as needed. The authors take full responsibility for the final text, data verification, scientific interpretations, and the overall integrity of the publication.

Conflicts of Interest: The authors declare no conflicts of interest.

References

1. Zhang, L.; Wang, X.; Yang, B.; Cai, J.; Yang, G.; Ma, H.; Du, C.; Liu, Z. Corrosion behavior and mechanisms of structural steels in industrial atmosphere of the Southwest Plateau, China. *J. Mater. Res. Technol.* **2026**, *42*, 4140–4153. [CrossRef]
2. Iwatt, M.U.; Akan, O.D.; Etim, I.N. Emerging mitigation techniques for microbially-influenced corrosion in the oil and gas industry. *Microbe* **2026**, *11*, 100702. [CrossRef]
3. Cunha, J.N.; Sampaio, M.T.; D'ELia, E.; Tribollet, B.; Mattos, O.R.; Almeida, T.C. The influence of CO_2 on the corrosion mechanism of carbon steel: New results and proposals. *Corros. Sci.* **2026**, *264*, 113729. [CrossRef]
4. Yang, J.; Tang, M.; Qiang, Y.; Li, X.; Deng, S. Chitosan-derived carbon dots for corrosion inhibition of cold rolled steel in 1.0 M HCl solution. *Colloids Surf. A Physicochem. Eng. Asp.* **2026**, *742*, 140478. [CrossRef]
5. Abdelli, L.; Nouadji, M.; Marmi, S.; Lekmine, F.; Chala, A.; Djouama, H. Multi-scale investigation of Eucalyptus globulus essential oil as a green corrosion inhibitor for C45 carbon steel in 1 M HCl: Experimental and computational study. *Surf. Interfaces* **2026**, *88*, 109087. [CrossRef]
6. Haddouchy, H.; Loughmari, S.; El Badaoui, H.; Mansour, A.A.; Dahbi, M.; Salghi, R.; El Bouadili, A.; Laouane, H.; Chtaini, A.; Najih, R.; et al. Elaboration, optimization, and characterization of new harmaline-based derivatives as corrosion inhibitors for E24 carbon steel in 1M HCl medium: An integrated experimental, surface, and computational approaches (DFT, MD, RDG, ELF). *J. Mol. Struct.* **2026**, *1363*, 145633. [CrossRef]
7. Mansour, A.A.; Loughmari, S.; Haddouchy, H.; Amarray, A.; Dahbi, M.; Salghi, R.; El Bouadili, A.; Laouane, H.; Chtaini, A.; Abdelatif, M.; et al. Evaluation of the performance of dioxadiazine derivatives as corrosion inhibitors for E24 carbon steel in 1 M HCl medium: Experimental approaches and theoretical simulations. *J. Mol. Liq.* **2026**, *442*, 129102. [CrossRef]
8. Bai, R.; Huang, W.; Zhao, F.; Zhu, L.; Wang, W.; Zhu, Y.; Ge, Y.; Wang, R. Symmetrical dibenzylimidazolium salts as corrosion inhibitors for carbon steel in 15% HCl: Experimental and theoretical studies. *Colloids Surf. A Physicochem. Eng. Asp.* **2026**, *738*, 139993. [CrossRef]
9. Deyab, M.A.; Mohsen, Q. Improved battery capacity and cycle life in iron-air batteries with ionic liquid. *Renew. Sustain. Energy Rev.* **2021**, *139*, 110729. [CrossRef]
10. Deyab, M.A.; Mohsen, Q.; Guo, L. Aesculus hippocastanum seeds extract as eco-friendly corrosion inhibitor for desalination plants: Experimental and theoretical studies. *J. Mol. Liq.* **2022**, *361*, 119594. [CrossRef]
11. Hafad, Y.; Benmenine, A.; Messaadia, L.; Benamira, M.; Mohamed, A.M.; Keffous, F.; Dizge, N. Eco-friendly corrosion inhibition of X52 carbon steel in HCl by Echinopsspinosus L. extract: Experimental and theoretical insights. *Colloids Surf. A Physicochem. Eng. Asp.* **2026**, *731*, 139092. [CrossRef]
12. Elharami, A.; El-Gheryby, Y.; Forsal, I.; Kerouad, S.; KotmanI, W.; Talfana, A.; Edaala, M.-A. Mechanistic insights into the eco-friendly corrosion inhibition of carbon steel in 1 M HCl by Origanum majorana extract: Electrochemical and theoretical study. *Next Mater.* **2026**, *11*, 101758. [CrossRef]

13. Pai, G.D.; Rajappa, S.K.; Rathod, M.R.; Kittur, A.A.; Mahesh, R.T. Eco-friendly corrosion protection of low-carbon steel by Macfadyena unguis-cati leaves extract: Chemical, electrochemical, and surface characterisation approaches. *Prog. Eng. Sci.* **2026**, *3*, 100267. [CrossRef]
14. Krishnanjana, K.; Ganesh, G.M. Efficacy of Punica granatum peel extract on thermo mechanically treated steel bar corrosion through electrochemical noise analysis. *Results Surf. Interfaces* **2026**, *23*, 100766. [CrossRef]
15. Torres, V.V.; Amado, R.S.; de Sá, C.F.; Fernandez, T.L.; Riehl, C.A.d.S.; Torres, A.G.; D'elia, E. Inhibitory action of aqueous coffee ground extracts on the corrosion of carbon steel in HCl solution. *Corros. Sci.* **2011**, *53*, 2385–2392. [CrossRef]
16. El-Saeed, H.M.; Fouda, A.; Deyab, M.; Shalabi, K.; Nessim, M.; El-Katori, E.E. Synthesis and characterization of novel ionic liquids based on imidazolium for acid corrosion inhibition of aluminum: Experimental, spectral, and computational study. *J. Mol. Liq.* **2022**, *358*, 119177. [CrossRef]
17. Okuma, S.O.; Obaseki, M. Integrated adsorption, kinetic–thermodynamic, and computational assessment of cestrum nocturnum as a green corrosion inhibitor for Carbon Steel in 1 M HCl. *Chem. Thermodyn. Therm. Anal.* **2026**, *21*, 100261. [CrossRef]
18. Sayed, A.G.; Ashmawy, A.M.; Elgammal, W.E.; Hassan, S.M.; Deyab, M.A. Synthesis, description, and application of novel corrosion inhibitors for CS AISI1095 in 1.0 M HCl based on benzoquinoline derivatives. *Sci. Rep.* **2023**, *13*, 13761. [CrossRef] [PubMed]
19. Deyab, M.A.; Słota, R.; Bloise, E.; Mele, G. Exploring corrosion protection properties of alkyd@lanthanide bis-phthalocyanine nanocomposite coatings. *RSC Adv.* **2018**, *8*, 1909–1916. [CrossRef] [PubMed]
20. Policarpi, E.D.B.; Spinelli, A. Application of *Hymenaeastigonocarpa* fruit shell extract as eco-friendly corrosion inhibitor for steel in sulfuric acid. *J. Taiwan Inst. Chem. Eng.* **2020**, *116*, 215–222. [CrossRef]
21. Wang, X.; Gu, Y.; Zhang, Q.; Xu, L.; Li, X. Rose, Gardenia, and *Solanum violaceum* extracts as inhibitors of steel corrosion. *Int. J. Electrochem. Sci.* **2019**, *14*, 8405–8418. [CrossRef]
22. Liu, Y.; Song, Z.; Wang, W.; Jiang, L.; Zhang, Y.; Guo, M.; Song, F.; Xu, N. Effect of ginger extract as green inhibitor on chloride-induced corrosion of carbon steel in simulated concrete pore solutions. *J. Clean. Prod.* **2019**, *214*, 298–307. [CrossRef]
23. Deyab, M.A.; El-Shamy, O.A.A.; Thabet, H.K.; Ashmawy, A.M. Electrochemical and theoretical investigations of favipiravir drug performance as ecologically benign corrosion inhibitor for aluminum alloy in acid solution. *Sci. Rep.* **2023**, *13*, 8680. [CrossRef] [PubMed]
24. Hammud, H.H.; Maache, S.A.; Al Otaibi, N.; Sheikh, N.S. An integrated experimental and theoretical studies on the corrosion inhibition of carbon steel by harmal extracts. *Molecules* **2022**, *27*, 7250. [CrossRef] [PubMed]
25. Vaidya, N.R.; Aklujkar, P.; Rao, R.R. Modification of natural gums for application as corrosion inhibitor: A review. *J. Coat. Technol. Res.* **2022**, *19*, 223–239. [CrossRef]
26. Deyab, M.A.; Mohsen, Q. Inhibitory influence of cationic Gemini surfactant on the dissolution rate of N80 carbon steel in 15% HCl solution. *Sci. Rep.* **2021**, *11*, 10521. [CrossRef] [PubMed]
27. Okuma, S.O.; Nwaeju-Okechukwu, C.C.; Oreko, B.U. Adsorption, kinetic, thermodynamic, thermal stability, and RSM optimization studies of Mitragyna speciosa as a green corrosion inhibitor for API 5 L X65 steel in aggressive oil and gas well treatment fluids. *Chem. Thermodyn. Therm. Anal.* **2026**, *22*, 100287. [CrossRef]
28. Tan, B.; Fu, A.; Guo, L.; Ran, Y.; Xiong, J.; Marzouki, R.; Li, W. Insight into anti-corrosion mechanism of Dalbergia odorifera leaves extract as a biodegradable inhibitor for X70 steel in sulfuric acid medium. *Ind. Crops Prod.* **2023**, *194*, 116106. [CrossRef]
29. Cookey, G.A.; Vopnu, T.; Maduelosi, J.N. Thermodynamic and kinetic studies of the corrosion inhibition of mild steel in 0.5 M HCl; using napoleonaeimperialis leaves extract. *J. Chem. Soc. Niger.* **2021**, *46*, 0474–0481. [CrossRef]
30. Chaudhary, S.; Tak, R.K.; Kumari, K.; Sharma, N. Thermodynamic and Kinetic Study of Corrosion Inhibition of Mild Steel by Plant Extract in Acidic Medium. *Mater. Int.* **2024**, *6*, 25. [CrossRef]
31. Lamghafri, S.; Daoudi, W.; Dagdag, O.; Naguib, I.A.; Nik, W.M.N.W.; Berisha, A.; Kim, H.; El Aatiaoui, A.; Zarrouk, A.; Lamhamdi, A. Promising corrosion resistance of mild steel, copper, and aluminum in hydrochloric acid solution using an environmentally friendly corrosion inhibitor. *J. Ind. Eng. Chem.* **2025**, *146*, 332–348. [CrossRef]
32. Deyab, M.A.; Ashmawy, A.M.; Nessim, M.I.; Mohsen, Q. New Gemini surfactants based on alkyl benzenaminium: Synthesis and links to application of corrosion protection. *J. Mol. Liq.* **2021**, *332*, 115855. [CrossRef]
33. Rahimi, A.; Farhadian, A.; Guo, L.; Akbarinezhad, E.; Sharifi, R.; Iravani, D.; Javidparvar, A.A.; Deyab, M.A.; Varfolomeev, M.A. Bio-based and self-catalyzed waterborne polyurethanes as efficient corrosion inhibitors for sour oilfield environment. *J. Ind. Eng. Chem.* **2023**, *123*, 170–186. [CrossRef]
34. Tran, H.N.; You, S.; Chao, H. Thermodynamic parameters of cadmium adsorption onto orange peel calculated from various methods: A comparison study. *J. Environ. Chem. Eng.* **2016**, *4*, 2671–2682. [CrossRef]
35. Yousif, Q.A.; Malhotra, S.S.; Bedair, M.A.; Ansari, A.; Hadi, A.K. Safflower plant extract as a sustainable corrosion inhibitor for carbon steel in acidic media: A combined electrochemical and computational study. *RSC Adv.* **2025**, *15*, 21006–21025. [CrossRef] [PubMed]

36. Zhang, Q.H.; Zhang, T.T.; Zhang, G.A. Synergistic mixture of Mori Cortex extract with KI as an eco-friendly compound corrosion inhibitor for carbon steel in acidic medium. *Colloids Surf. A Physicochem. Eng. Asp.* **2025**, *725*, 137670. [CrossRef]
37. Gharbi, A.; Dridi, M.; Rémazeilles, C.; Hamlaoui, Y.; Pedraza, F. Eco-friendly corrosion inhibition and antioxidant potential of Ficus elastica leaf extract for C1020 carbon steel in acidic medium. *Mater. Today Commun.* **2025**, *47*, 113157. [CrossRef]
38. Maizia, R.; Djermoune, A.; Amoura, D.; Zaabar, A.; Thomas, A.; Dib, A.; Martemianov, S. Bidens aureaaiton plant extract as a green and sustainable corrosion inhibitor for carbon steel X42 in hydrochloric acidic medium: Experimental and computational studies. *Mater. Chem. Phys.* **2025**, *339*, 130740. [CrossRef]
39. Deyab, M.A.; Abdeen, M.M.; Hussien, M.; El-Sayed, I.E.; Galhoum, A.; El-Shamy, O.A.A.; Elfattah, M.A. Novel corrosion inhibitor for carbon steel in acidic solutions based on α-aminophosphonate (chemical, electrochemical, and quantum studies). *Molecules* **2023**, *28*, 4962. [CrossRef] [PubMed]
40. Lakikza, I.; Benguerba, Y.; Boublia, A.; Aouni, S.I.; Lahbib, H.; Ferkous, H.; Ghodbane, H.; Benamor, Y.; Bentalib, A.S.; Ernst, B. Comprehensive evaluation of Alysicarpus compactum extract as a natural corrosion inhibitor for St37 carbon steel in acidic media. *J. Ind. Eng. Chem.* **2025**, *147*, 161–178. [CrossRef]

Disclaimer/Publisher's Note: The statements, opinions and data contained in all publications are solely those of the individual author(s) and contributor(s) and not of MDPI and/or the editor(s). MDPI and/or the editor(s) disclaim responsibility for any injury to people or property resulting from any ideas, methods, instructions or products referred to in the content.